

ORIGINAL RESEARCH PAPER

Polyvinylpyrrolidone and Brij-35 Stabilized IrO₂ Nanoclusters As Highly Effective Catalyst In The Degradation Of Acid Orange 10: A Comparative Study

Rajni Lasyal^{*1} Shakunj Rajput²

¹Department of Chemistry, Rajkiya Mahavidyalaya, Chinyalisaur, Uttarkashi, Uttarakhand, India.

²Department of Chemistry, Government Degree College Bhupatwala, Hardwar, Uttarakhand India.

Received: 2022-12-08

Accepted: 2023-03-31

Published: 2023-05-16

ABSTRACT

In this study, the degradation of azo-dye acid orange 10 (AO 10) has been investigated using Polyvinylpyrrolidone (PVP) and Polyoxyethylene Lauryl Ether (Brij-35) stabilized Iridium oxide (IrO₂) nanoclusters as catalysts. A simple chemical reduction method was used to synthesize the above-mentioned nanoclusters. The characteristics of the nanocatalysts were determined by UV-visible spectrophotometer, TEM, and XRD. The kinetic study has been carried out at λ_{max} of the reaction mixture i.e. 479 nm spectrophotometrically. The degradation follows first-order kinetics concerning oxidant and catalyst concentration while an order is one at lower substrate concentration tending towards zero at higher concentration. The degradation kinetics has been supported by the derived rate law. The results showed that PVP-stabilized IrO₂ nanoclusters outperformed Brij-35 stabilized IrO₂ nanoclusters, exhibiting the fastest degradation rate. The progress of the degradation process was monitored by UV-vis spectroscopy. Using PVP-stabilized IrO₂ nanoclusters as a catalyst is a very promising approach for the remediation of acid orange 10 due to the fast degradation rate and high degradation efficiency. In addition, PVP-stabilized IrO₂ nanoclusters can be easily recovered and recycled for three consecutive cycles. It can be inferred from this study that catalytic oxidation methods are active and environment-friendly for the remediation of dyes.

Keywords: Degradation, Kinetics, PVP, Brij-35, Rate law, Acid orange10

How to cite this article

Lasyal R., Rajput S., Polyvinylpyrrolidone and Brij-35 Stabilized IrO₂ Nanoclusters As Highly Effective Catalyst In The Degradation Of Acid Orange 10: A Comparative Study. J. Water Environ. Nanotechnol., 2023; 8(2): 108-120
DOI: 10.22090/jwent.2023.02.002

INTRODUCTION

Synthetic dyes have been widely used in various fields, especially in the textile and printing industries. Azo dyes which constitute a significant proportion of synthetic dyes pose a significant threat to the environment and eco-biology because of their non-biodegradability and potential genotoxic and carcinogenic nature [1,2]. Dye removal or degradation from wastewater has been extensively studied to reduce its impact on the environment [3,4]. Several physicochemical and

biological methods, such as adsorption, ozonation, photocatalysis, Fenton, reductive and oxidative degradation, and two or more combination methods have been successfully applied to the treatment of various dyes [5-7].

Among these methods, oxidative degradation is a fast, simple, and low-cost method, which is easy to implement in industries for the degradation of dyes [8]. Conventional chemical oxidation of dyes typically involves the use of oxidizing agents such as chlorine in the form of sodium hypochlorite, ozone (O₃), hydrogen peroxide, and permanganate

* Corresponding Authors Email: lasyal.rajni@gmail.com



This work is licensed under the Creative Commons Attribution 4.0 International License.

To view a copy of this license, visit <http://creativecommons.org/licenses/by/4.0/>.

[9]. Chlorination and ozonation have slower rates and high operating costs and limited effects on carbon content [10,11]. Therefore, during the last decade, special attention has been focused on the studies concerning the use of advanced oxidation processes (AOPs) utilizing Fenton and photo-assisted Fenton reactions for azo dye degradation [12]. Their effectiveness results from the generation of highly reactive hydroxyl radicals (OH[•]) that decolorize both soluble and insoluble dyes. However, the generation of large volumes of iron sludge is a major demerit of the process. There are reports for the use of metal nanoparticles in azo dye remediation, including nano zero-valent iron, (NZVI) [13, 14] and iron-based bimetallic nanoparticle, such as Fe/Ni [15]. Recently, Iridium (Ir) nanoparticles have emerged as a promising agent to treat azo dyes [16].

Oxidation by iron(III) in the form of various complexes has received much attention presumably due to its easy availability, less complexity involved in the oxidation, and its ability to act in acidic and alkaline medium both [17]. In this paper, a very fast oxidative degradation method for acid orange 10 (AO 10) based on novel PVP and Brij-35 stabilized IrO₂ nanoclusters as nanocatalysts using Hexacyanoferrate(III) abbreviated as HCF(III) ions as an oxidant has been reported. The degradation study has been monitored by UV-vis spectrophotometer showing the decrease in absorbance with the decrease in the concentration of dye with time. The comparison of the catalytic activity of PVP stabilized & Brij-35 stabilized IrO₂ nanoclusters with IrCl₃ proves their use as potential catalysts in the oxidative degradation of dyes. Recycling catalysts and calculation of turnover frequency is also important feature of this work.

The major advantage of IrO₂ nanoparticles over other catalysts is their superior selectivity and efficiency in degrading pollutants. IrO₂ nanoclusters can effectively break down pollutants into simpler and more harmless compounds, while other catalysts may simply convert pollutants into different forms of pollutants [18]. Additionally, IrO₂ nanoparticles are more stable in harsh environmental conditions and have longer lifespans compared to other catalysts. IrO₂ nanoclusters are known to have excellent catalytic activity due to their high surface area and their ability to form strong bonds with other molecules [19].

This is the first study to compare the catalytic performance of PVP and Brij-35 stabilized IrO₂

nanoclusters. The results indicate that PVP and Brij-35 stabilized IrO₂ nanoclusters have superior catalytic performance compared to other catalysts, such as activated carbon, for the degradation of Acid Orange 10. This research work provides new insight into the catalytic performance of PVP and Brij-35 stabilized IrO₂ nanoclusters for the degradation of organic pollutants.

MATERIALS AND METHODS

Materials and chemicals

All the chemicals used in the fabrication of iridium oxide nanoclusters and degradation of acid orange 10 were of analytical grade. Iridium chloride (IrCl₃.xH₂O, 99.6%), the precursor for the synthesis of IrO₂ nanoclusters was purchased from Loba Chemie Pvt. Ltd. Mumbai, India. Hexacyanoferrate(III) purchased from Merck was recrystallized before use. A fresh solution was placed in amber-colored bottles to prevent photodecomposition as the aqueous solution of HCF(III) tends to get hydrolyzed in light. A fresh solution was prepared for each set of variations to get better results.

Acid orange 10 (C₁₆H₁₀N₂Na₂O₇S₂, pure, certified) was obtained from SRL Pvt. Ltd, India. Additionally, stabilizers, Polyvinylpyrrolidone (PVP) and Brij-35 were procured from Merck and Thomas Baker respectively. Potassium dihydrogen phosphate (KH₂PO₄, 99.0%) and Sodium Hydroxide (NaOH, extra pure) were used to maintain the pH of the reaction mixture

Synthesis of iridium nanoclusters

The PVP and Brij-35 stabilized IrO₂ nanoclusters were synthesized by the wet reduction method as reported previously [20] as depicted in Fig. 1. The reaction was administered in a three-necked flask. A calculated amount of precursor solution (7.07 × 10⁻⁴ mol dm⁻³) was prepared in methanol, which was added to the pre-prepared solution of stabilizer (PVP/Brij-35) in water at room temperature with continuous stirring. 1 ml NaOH (0.2M) solution was added to the solution of precursor and stabilizer solution dropwise with vigorous stirring for 15 min to obtain a colorless solution. The solution was further agitated for 15 min before refluxing for 2 hours in an oil bath. A series of color changes were witnessed before the fabrication of IrO₂ nanoclusters. Finally, the blackish-brown colloidal dispersion of iridium nanoclusters was obtained without any precipitation. There was an

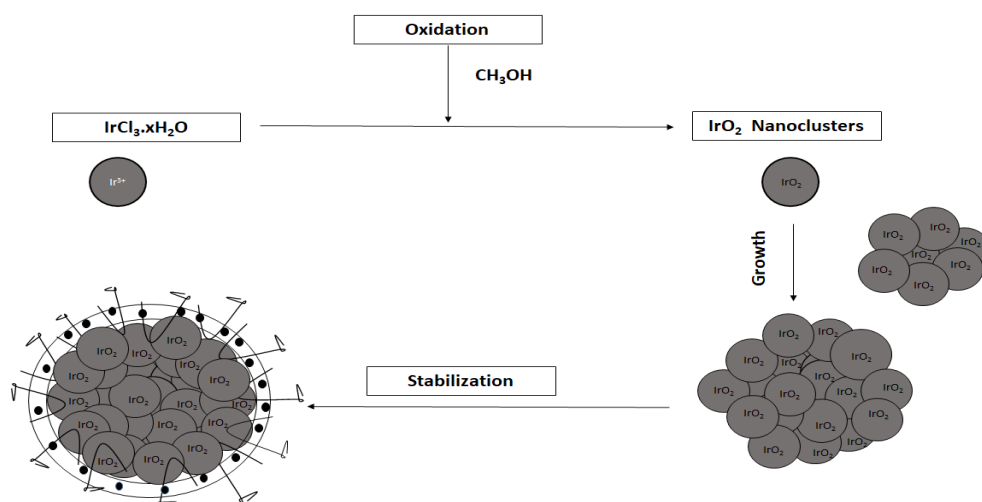


Fig. 1: Schematic presentation of redox reaction during the fabrication of IrO₂ nanoclusters with PVP and Brij-35 using methanol as a reducing agent

increase in the temperature from 30 °C to 80 °C during synthesis which tends to become constant after the fabrication of IrO₂ nanoclusters.

Degradation of acid orange 10

The PVP and Brij-35 stabilized IrO₂ nanoclusters were used as catalysts for the acid orange 10 degradation at optimal pH (8.0) and temperature (40 ± 1°C). The thermostat fixed to a rotator, rotating at 10 rpm was used to attain thermal equilibrium and maintain solution uniformity during the degradation process. The requisite amount of each reactant was thoroughly mixed in a 250 ml iodine flask. Acid orange 10 solutions were added to the aforementioned reaction mixture containing a weighed amount of HCF(III), buffer, and IrO₂ nanoclusters to initiate the degradation. The reaction was monitored by measuring the UV-vis absorption spectra of the sample solution taken out at regular intervals (0, 5, 10, 15, 20, 30, 45, and 60 min at λ_{\max} of the reaction mixture i.e. 479 nm. With time there was a gradual decrease in the absorbance of the dye showing its degradation. A kinetic study of the degradation process was determined by the initial rate method.

Instruments and Characterization

The XRD pattern of measurement was carried out using dried powder by Bruker AXS D-8 Advance diffractometer with monochromatized Cu K α (λ = 0.154 nm) radiation, 230 V, 50Hz, 6–5 kV A, scan rate 1° min⁻¹ operating with a range of 2 θ angles from 10° to 70°. The approximate particle size

was determined by the Debye–Scherrer equation. Transmission electron microscopy (TEM) imaging was performed using an FEI-TECHNAIG-20 transmission electron microscope operated at 200 kV. TEM samples were prepared by placing a drop of the nanoparticle suspension in ethanol on a piece of TEM grid and drying under ambient conditions. A UV/Vis spectrophotometer (Systronics-117) was utilized to collect the absorption spectra of azo dye degradation. The pH value was measured by a digital pH meter (Systronics μ -pH System 361).

RESULTS AND DISCUSSION

Nanoclusters

Table 1 shows the comparison of synthesis conditions and particle size of IrO₂ nanoclusters formed with PVP and Brij-35 which is well supported by the XRD patterns shown in Fig. 2. The approximate particle size of the IrO₂ nanoclusters was determined by employing the Scherrer equation:

$$D = \frac{0.9\lambda}{\cos\theta \beta}$$

where D is the average particle size of IrO₂ nanoclusters, λ is the wavelength of incident X-ray (corresponding to 0.154 nm), θ is the position of diffraction peak as well as Bragg's angle, β corresponds to full-width at half maxima of the diffraction peak, FWHM (in radian). It is observed that the diffractogram of IrO₂ nanoclusters formed with PVP is quite different from that of IrO₂ nanoclusters formed with Brij-35. The PVP-stabilized IrO₂ nanoclusters are amorphous with

Table 1: Synthesis conditions and particle size of IrO₂ nanoclusters

S. No.	Precursor	Solvent/ Reductant	Stabilizer	Precursor: Stabilizer (w/w)	NaOH	Reflux Time	Approximate particle size (nm)	
							XRD	TEM
(a)	IrCl ₃ .xH ₂ O	Methanol	PVP	1:25	1ml	2 h	4.12, 4.71	4.05 ± 0.25
(b)	IrCl ₃ .xH ₂ O	Methanol	Brij-35	1:25	1ml	2 h	17.02, 18.82, 25.71	36.36 ± 1.0

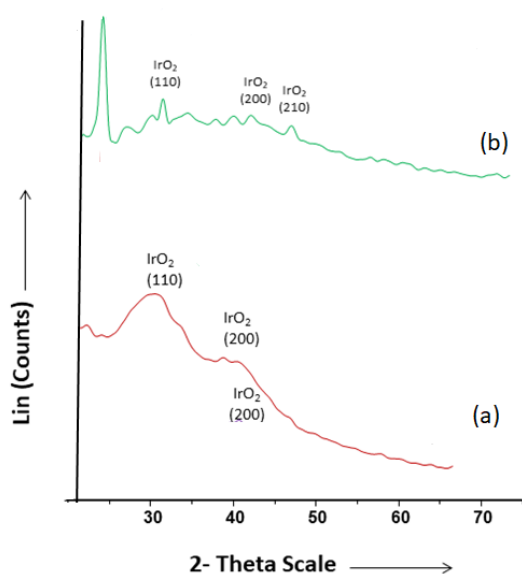


Fig. 2: XRD patterns of (a) PVP stabilized nanoclusters (b) Brij-35 Stabilized nanoclusters (JCPDS card no. 15870) as represented in Table 1

broad peaks characteristic of materials with small size while Brij-35 stabilized IrO₂ nanoclusters are crystalline in nature and larger in size. This may be attributed to the steric effect and chemical bonding of stabilizers on the particle size. The stabilization of colloidal metal particles with polymers in water is often discussed by the adsorption of the polymer on these particles. These large adsorbates provide a steric barrier that prevents close contact of metal nanoclusters to each other. The interaction between the surface of the metal particles and the polymers is considered to be hydrophobic. However, coordination of the polymer to metal particles has been proposed by the shift of the >C=O stretching in the IR spectra of the PVP and surrounding nanoclusters. PVP may play the same role for Au and other noble metal nanoparticles (IrO₂ nanoclusters). The large particle size and less stability of Brij-35 capped IrO₂ may be due

to less interaction of the train part of Brij -35 and nanoclusters [20] Fig. 3(a) is the TEM image of PVP-stabilized IrO₂ nanoparticles with a diameter of 4.05 ± 0.25 nm; Fig. 3(b) shows the TEM image of Brij-35 stabilized IrO₂ nanoparticles having a diameter of 36.36 ± 1.0 nm. Under the same reaction conditions, the particle size of PVP-stabilized IrO₂ nanoclusters is nine times smaller than the IrO₂ nanoclusters formed with Brij-35. TEM images demonstrate that IrO₂ nanoclusters have an agglomeration tendency and are larger as compared to PVP-stabilized IrO₂ nanoclusters.

Comparison of degradation kinetics of AO 10

The comparison of catalytic activity of PVP-stabilized IrO₂ nanoclusters and Brij-35 stabilized IrO₂ nanoclusters has been studied by kinetic-spectrophotometric method in the oxidation of AO 10 dye by hexacyanoferrate(III) ions in an aqueous alkaline medium. The reactions have been carried out at a constant pH and a constant temperature ($40 \pm 1^\circ\text{C}$) at different concentrations of one reactant keeping the concentration of the other constant.

Influence of pH

pH of the reaction mixture is the most important factor that affects the degradation kinetics of azo dyes. When it comes to ionic reactions (here, AO 10 moieties and other reactants), the pH has an impact on ionization; hence, the ideal pH value for ionization is required, and the rate of reaction is then evaluated at that optimum pH value. By altering the pH of the solution from 6.0 to 9.5, the effect of pH on AO 10 degradation in a catalyst-mediated system was investigated. The most favorable pH for the breakdown of AO 10 is 8.0, displaying the maximum ionization, as seen in Fig. 4. According to studies in the literature, OH⁻ combines with dyes in an alkaline medium to extract proton (H⁺) and generates anionic species

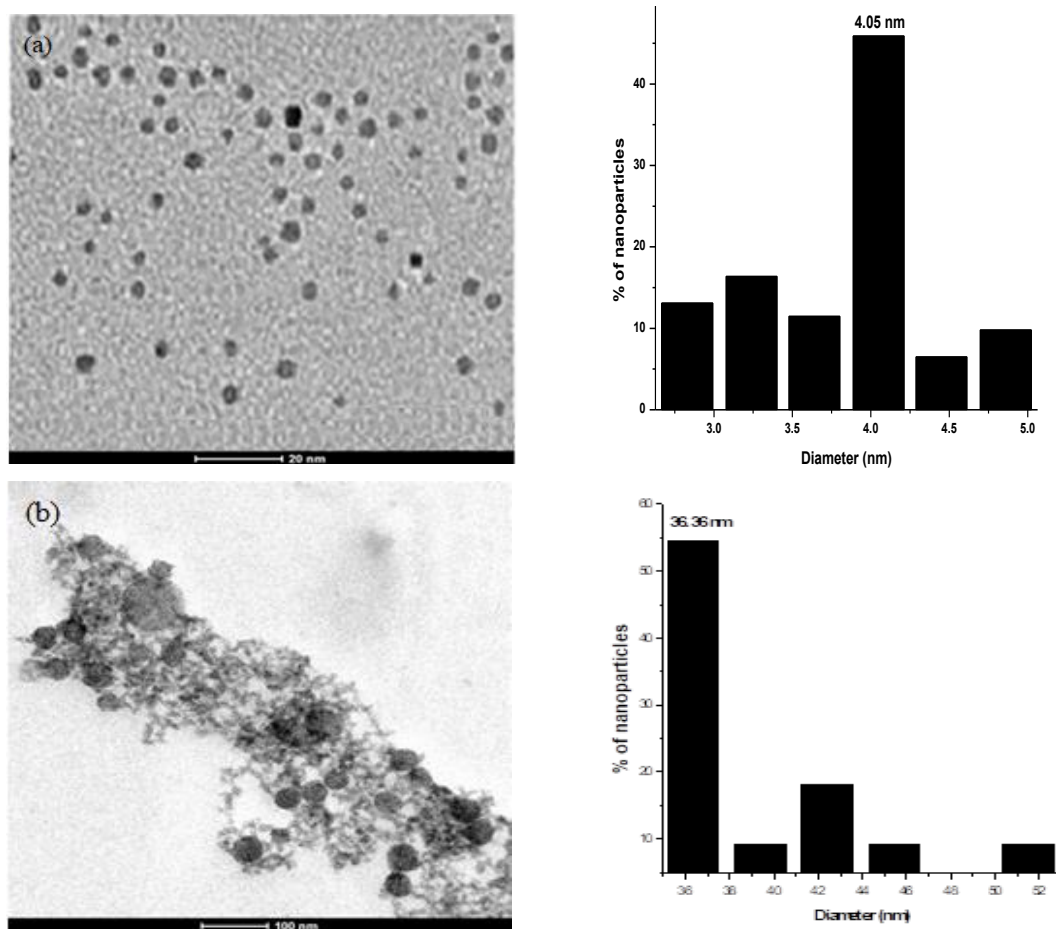


Fig. 3: TEM micrographs and corresponding particle size distribution histograms of (a) PVP-stabilized IrO₂ nanoclusters and (b) Brij-35 stabilized IrO₂ nanoclusters.

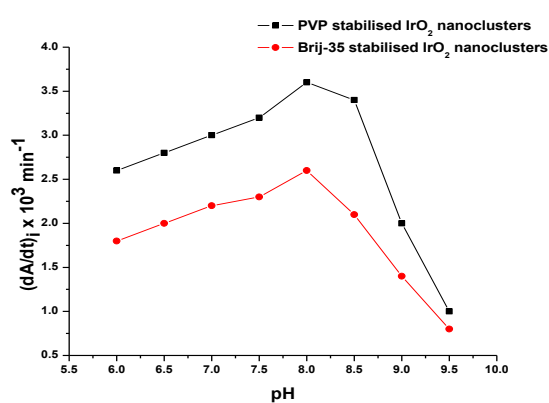


Fig. 4: Effect of pH on the degradation rate of AO 10 by HCF(III). Experimental conditions: [AO 10] = $3.0 \times 10^{-5} \text{ mol dm}^{-3}$; [HCF(III)] = $3.0 \times 10^{-6} \text{ mol dm}^{-3}$; [IrO₂ nanoclusters] = $1.004 \times 10^{-7} \text{ mol dm}^{-3}$; Temperature = $40 \pm 0.1^\circ\text{C}$.

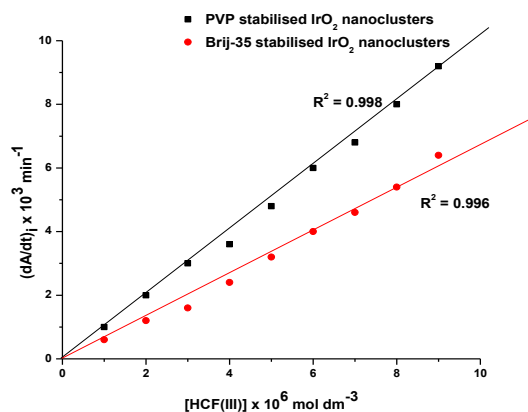


Fig. 5: Effect of [HCF(III)] on the degradation rate of AO 10 by HCF(III). Experimental conditions: [AO 10] = $3.0 \times 10^{-5} \text{ mol dm}^{-3}$; [IrO₂ nanoclusters] = $1.004 \times 10^{-7} \text{ mol dm}^{-3}$; pH=8.0; Temperature = $40 \pm 0.1^\circ\text{C}$.

Table 2: Reaction rate and k_1 of reactions catalyzed by PVP-stabilized IrO₂ nanoclusters and Brij -35 stabilized IrO₂ nanoclusters

	<i>IrCl₃ catalyzed</i>	<i>Brij-35 stabilized IrO₂ nanoclusters</i>	<i>PVP stabilized IrO₂ nanoclusters</i>
	<i>reaction</i>	<i>catalyzed reaction</i>	<i>catalyzed reaction</i>
$(da/dt)_i \times 10^3$	1.8	2.4	3.0
(min^{-1})			
k_1 (calculated) $\times 10^6$	6.90	8.44	10.74
(sec^{-1})			

of dye in equilibrium, which can be assured by the proposed degradation mechanism. Because of the coulombic repulsion between anionic dye surface and OH⁻ ions, oxidation of organic compounds may decrease after reaching the optimal pH value [16].

Effect of oxidant concentration

Fig. 5 shows the kinetics of the oxidative removal of azo dye AO10 by HCF(III) using PVP-stabilized IrO₂ nanoclusters and Brij-35 stabilized IrO₂ nanoclusters as catalysts. The statistics indicate how the concentration of HCF(III) ions affects the reaction rate. The results show that AO 10 oxidation follows first-order kinetics concerning [HCF(III)]. It can be seen that rate of degradation of AO 10 degradation rate increases as the concentration of HCF(III) increases. HCF(III) ions were present in concentrations ranging from 1.0×10^{-6} to 9.0×10^{-6} mol dm⁻³.

Effect of dye concentration

It is crucial to look into the relationship between the initial dye concentration and the rate of degradation from an application standpoint. By altering the concentration of AO 10 from 1×10^{-5} to 9×10^{-5} mol dm⁻³, the effect of dye concentration change was investigated. Fig. 6 depicts the first-order rate dependency on lower substrate concentrations, which tends to be zero order at larger concentrations i.e at low concentrations of dye, there is a steep increase in the rate of reaction with increasing dye concentration and the rate at which product can be formed is limited by the concentration of substrate available but as the concentration of dye increases, adding more substrate will not affect the rate of the reaction in any significant manner.

Effect of catalyst concentration

Because the quantity of catalyst can influence the rate of dye degradation, the concentration of IrO₂ nanoclusters was adjusted several times, ranging from 0.2×10^{-7} to 1.204×10^{-7} mol dm⁻³. As illustrated in Fig. 7, first-order kinetics concerning PVP-stabilized IrO₂ nanoclusters and Brij-35 stabilized IrO₂ nanoclusters are revealed by a progressive increase in rate with their concentration. The increased rate indicates that the mass of the catalyst may have influenced the reaction rate.

Comparison of catalytic degradation efficiency of PVP-stabilized IrO₂ nanoclusters and Brij-35 stabilised IrO₂ nanoclusters

Under comparable experimental settings, the influence of particle size of PVP-stabilized IrO₂ nanoclusters and Brij-35 stabilized IrO₂ nanoclusters on the rate of degradation of AO 10 was investigated. Table 2 and Fig. 8 demonstrate the degradation rate for the reaction catalyzed by IrCl₃, PVP-stabilized IrO₂ nanoclusters and Brij-35 stabilized IrO₂ nanoclusters. The rate is the highest for PVP-stabilized IrO₂ nanoclusters when compared to other catalysts. This shows that PVP-stabilized IrO₂ nanoclusters had higher catalytic activity than Brij-35 stabilized IrO₂ nanoclusters and IrCl₃. It is possible due to the large surface area to volume ratio of the PVP-stabilized IrO₂ nanoclusters as compared to other catalysts.

Effect of Temperature on the reaction rate

In the present study, the effect of temperature on the oxidation of acid orange 10 at optimum pH in the presence of both, PVP-stabilized IrO₂ nanoclusters and Brij-35 stabilized IrO₂ nanoclusters has been studied at four different temperatures - 40, 45, 50,

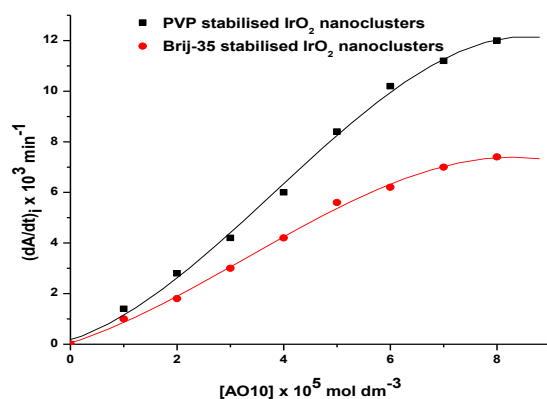


Fig. 6: Effect of [AO 10] on the degradation rate of AO 10 by HCF(III). Experimental conditions: [HCF(III)] = $3.0 \times 10^{-6} \text{ mol dm}^{-3}$; [IrO₂ nanoclusters] = $1.004 \times 10^{-7} \text{ mol dm}^{-3}$; pH=8.0; Temperature = $40 \pm 0.1^\circ\text{C}$.

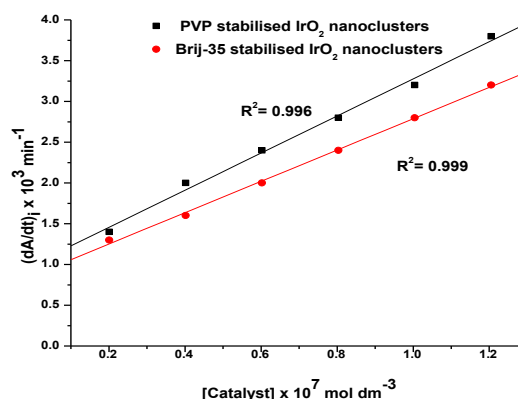


Fig. 7: Effect of [catalyst] on the degradation rate of AO 10 by HCF(III). Experimental conditions: [HCF(III)] = $3.0 \times 10^{-6} \text{ mol dm}^{-3}$; [AO 10] = $3.0 \times 10^{-5} \text{ mol dm}^{-3}$; pH=8.0; Temperature = $40 \pm 0.1^\circ\text{C}$.

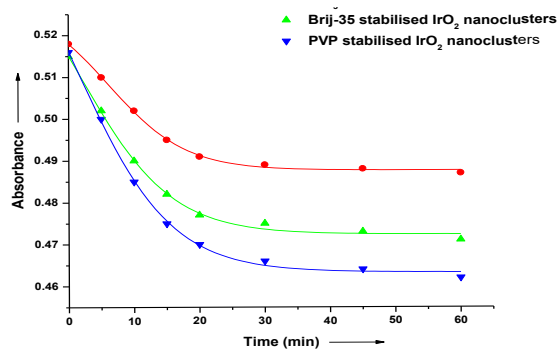


Fig. 8: Absorbance vs time plots for the comparative study of [catalyst] on the oxidation of acid orange 10. Experimental conditions: [HCF(III)] = $3.0 \times 10^{-6} \text{ mol dm}^{-3}$; [AO 10] = $3.0 \times 10^{-5} \text{ mol dm}^{-3}$; [IrO₂ nanoclusters] = $1.004 \times 10^{-7} \text{ mol dm}^{-3}$; pH=8.0; Temperature = $40 \pm 0.1^\circ\text{C}$.

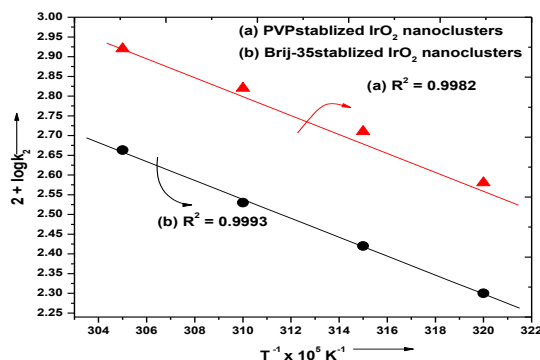


Fig. 9: Arrhenius plot for oxidation of acid orange 10 with (a) PVP stabilized IrO₂ nanoclusters (b) Brij-35stabilized IrO₂ nanoclusters

and 55°C . The observations have been made under identical conditions at different temperatures taking the specific runs for each catalyst. The first order rates constant ' k_1 ' were evaluated by the slope of $\log(a-x)$ vs time plots. The first order rate constant thus evaluated was divided by $[S]$ to get the second order rate constant k_2 . A plot of $\log k_2$ versus $1/T$ was linear showing that the Arrhenius equation was followed as shown in Fig. 9.

Recycling of catalysts and turnover frequency

The lifespan of PVP-stabilized IrO₂ nanoclusters was utilized to evaluate the economy of the current oxidative degradation process, which is the number of times a catalyst may be reused without compromising its efficiency. For three cycles, these nanoclusters were retrieved

and reused. The treated reaction mixture was centrifuged after the first degradation cycle. The generated nanoclusters were rinsed five to six times with double distilled water before being utilized as a catalyst in the kinetic investigation. For two consecutive cycles with fixed experimental circumstances, the same procedure was used. Table 3 summarises the findings. The rate of reaction was discovered to be decreasing with each subsequent cycle. The persistent agglomeration of IrO₂ nanoclusters after each cycle is, nevertheless, responsible for the progressive decline in catalytic efficacy. Fig.10, the XRD pattern of recovered nanoclusters after the first, second, and third cycles depict the increase in size of IrO₂ nanoclusters after each cycle.

Table 3: Turnover frequency, Particle size, and k_1 of PVP-stabilized IrO₂ nanoclusters before and after recovery up to three consecutive cycles

S. No	No. of cycles	(dn/dt) × 10 ⁻¹⁸ (molecules/s)	Approximate Particle size (nm)	TOF (s ⁻¹)	k_1 × 10 ⁵ (s ⁻¹)
1.	Before recovery	55.47	4.05	5.48	9.21
2.	After I cycle	46.19	9.40	1.96	7.67
3.	After II cycle	41.55	26.46	0.63	6.90
4.	After III cycle	32.34	33.81	0.38	5.37

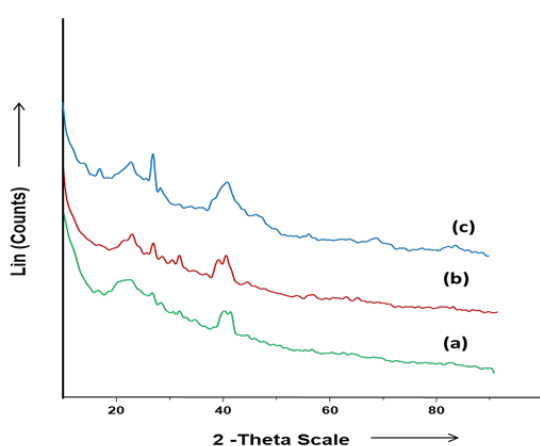


Fig. 10: XRD patterns of PVP stabilized nanoclusters (a) First cycle (b) Second cycle (c) Third cycle

The values of turnover frequency (TOF) given in Table 3 reveal that the catalytic activity of PVP-stabilized IrO₂ nanoclusters decreased significantly with each successive cycle. These nanoclusters increase in size (because of Ostwald ripening) after each cycle, which accounted for TOF calculations in each cycle [21].

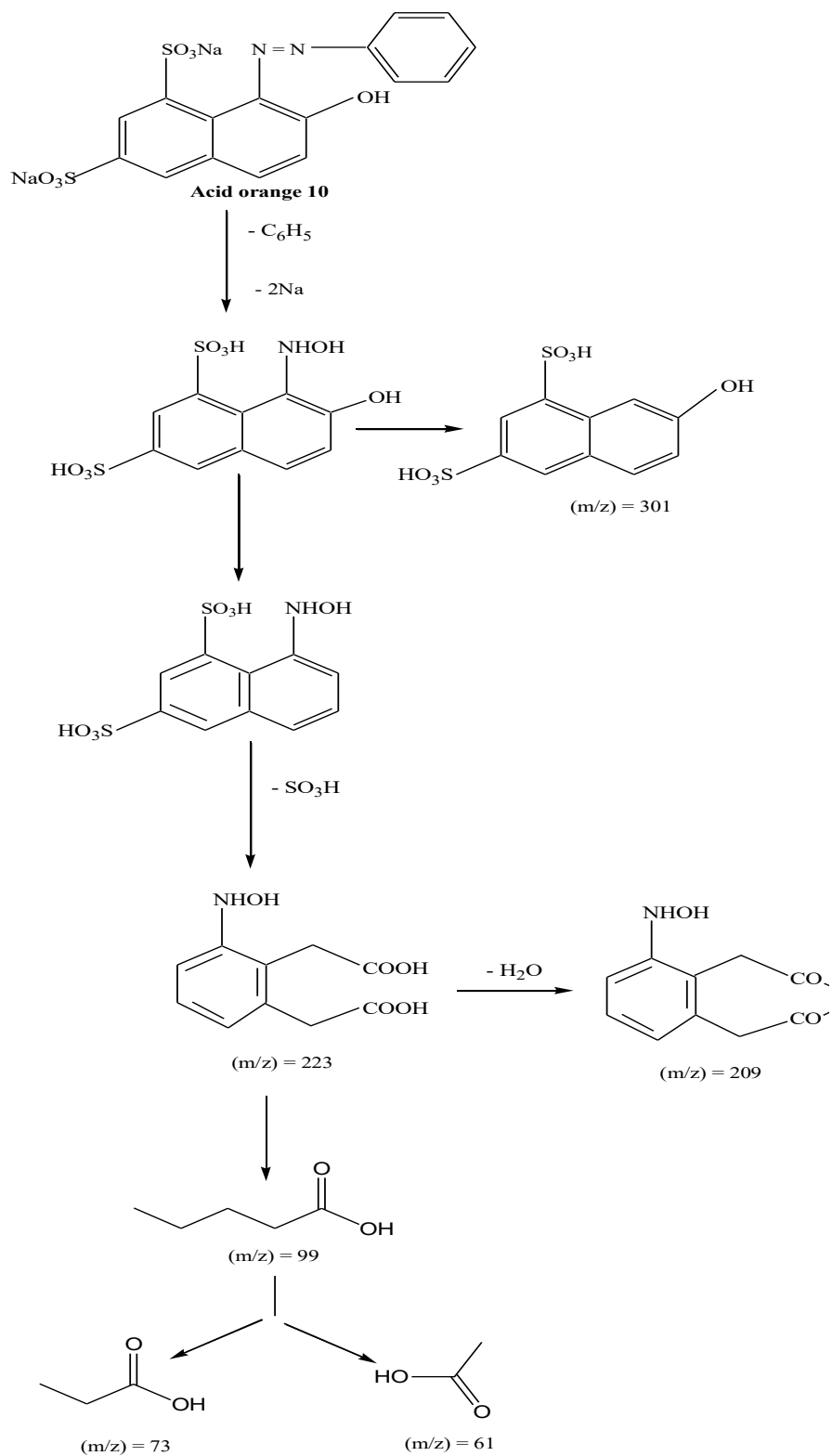
Proposed degradation Pathway of AO10

The UV-vis spectrum of acid orange 10 was recorded from 220 to 700 nm using a UV-vis spectrophotometer (Systronics -117) with a spectrometric quartz cell (1cm path length). The maximum absorbance wavelength (λ_{max}) was found at 479 nm which is attributed to $n \rightarrow \pi^*$ transition related to the $-N=N-$ group in the acid orange 10 molecule [22, 23]. Therefore, the concentration of acid orange 10 in the reaction mixture at different times was determined by measuring the absorption intensity of the solution

at 479 nm and using the calibration curve. Fig. 11 confirms the successful degradation of acid orange 10. Initially, the spectrum corresponds to a broad band at 479 nm for acid orange 10. The intensity of this peak decreased with time and a new peak appeared at 241 nm suggesting that the chromophore responsible for the color of the dye ($-N=N-$) was broken leading to the degradation of a substrate to new product/products.

The identification of extracted product/products was performed by Liquid chromatography-mass spectrometry (LC-MS) (BRUKER, ELITE) using C₁₈ column with acetonitrile: water (1:1) as mobile phase at a flow rate of 300 μ L/min. LC-MS spectra of the extracted product/products given in Fig. 12 indicate the formation of anticipated 3-(hydroxyamino) benzene -1,2-diethanoic acid, 3-(hydroxyamino) benzene-1,2-diethanoic anhydride and 5-hydroxy naphthalene -1, 3- disulphonic acid as minor degradation products and pentanoic acid, propanoic acid, ethanoic acid as major degradation products which are simple and less hazardous.

The products, depicted in the proposed degradation pathway (Scheme 1) arise from the indiscriminate attack of OH⁻ ions at various sites on the dye molecule. The formation of hydroxylated products mainly arises from the attack of hydroxyl ions on the dye surface [15]. Initially, more active bonds are hydroxylated. This includes the C-N bond linked to the benzene or naphthalene ring and C-S bond of the sulfate group linked to the naphthalene ring or the benzene ring, to form organic acids with or without hydroxyl group and the related ions (SO₄²⁻ and NH₄⁺). These aromatic acids are subsequently hydroxylated and lead to the cleavage of the aromatic ring to form aliphatic acids [12].



Scheme 1: Proposed degradation pathway for acid orange 10

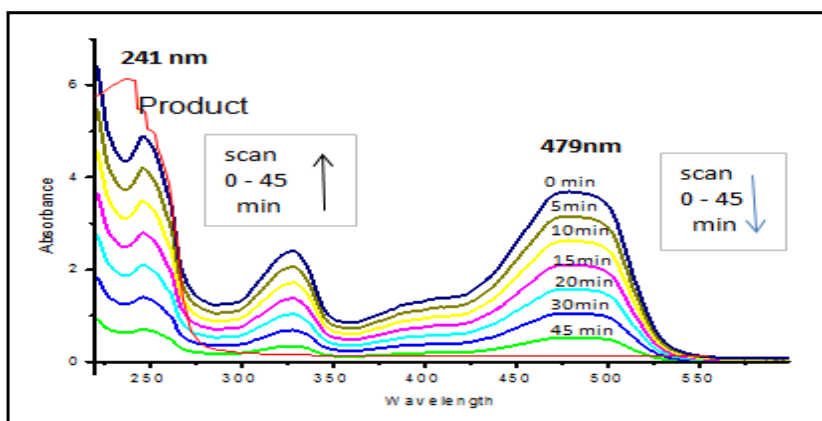


Fig. 11: UV-vis spectra showing the degradation of acid orange 10.

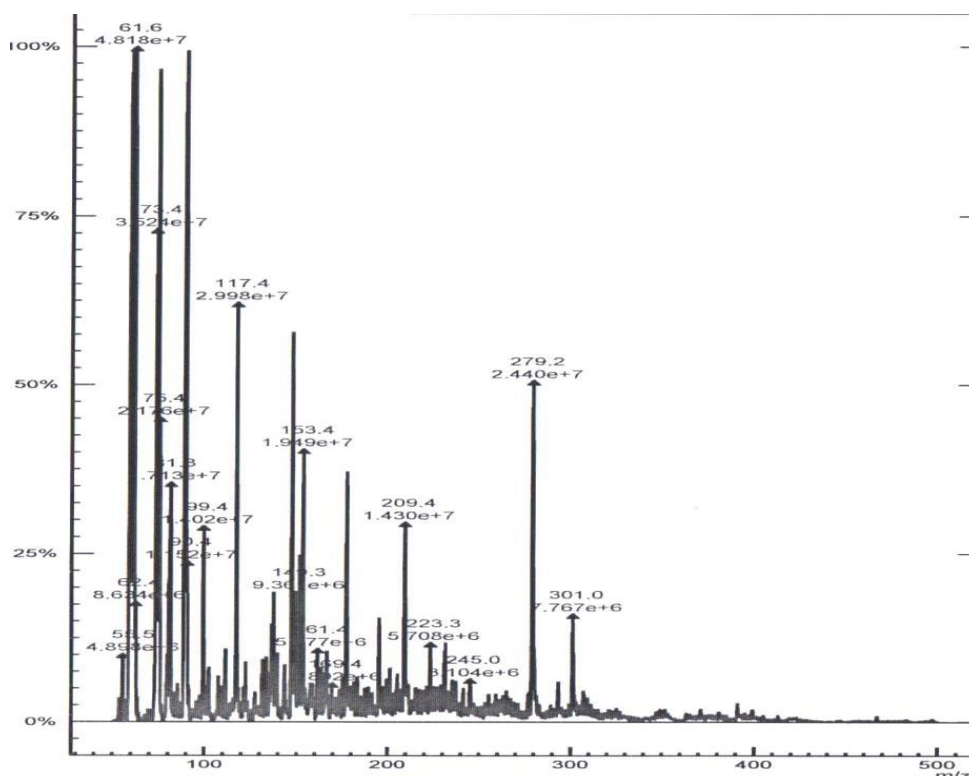


Fig. 12: LC-MS spectra showing the degradation of acid orange 10.

Mechanism

Though it is impossible to propose a mechanism for such a complicated reaction the experimental results and previous evidence lead us to propose a mechanism for the aforementioned electron transfer reaction which involves binding of substrate to the surface of IrO₂ nanoclusters (Ir_n) and then reacting with HCF(III) ions present in solution.

In Scheme 2, acid orange 10 is believed to exist as an anion, D⁻ in an alkaline medium where it forms a loosely bonded complex with IrO₂ nanoclusters (Ir_n). This complex slowly reacts with HCF(III) ion, yielding Ir_n and Fe(CN)₆⁴⁻ as products [21]. It has been claimed that the metal ion complexing with organic substrate facilitates electron transport. The formation of the complex was also proved kinetically by the Michaelis-Menton plot i.e. a

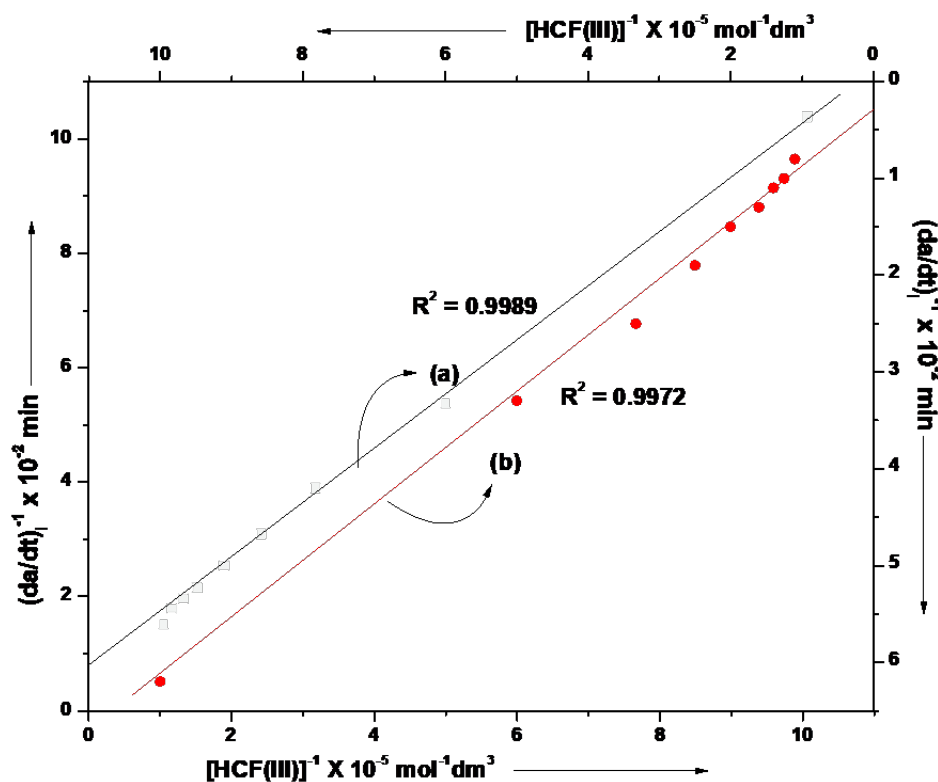


Fig. 13: Plot of rate⁻¹ vs [HCF(III)]⁻¹

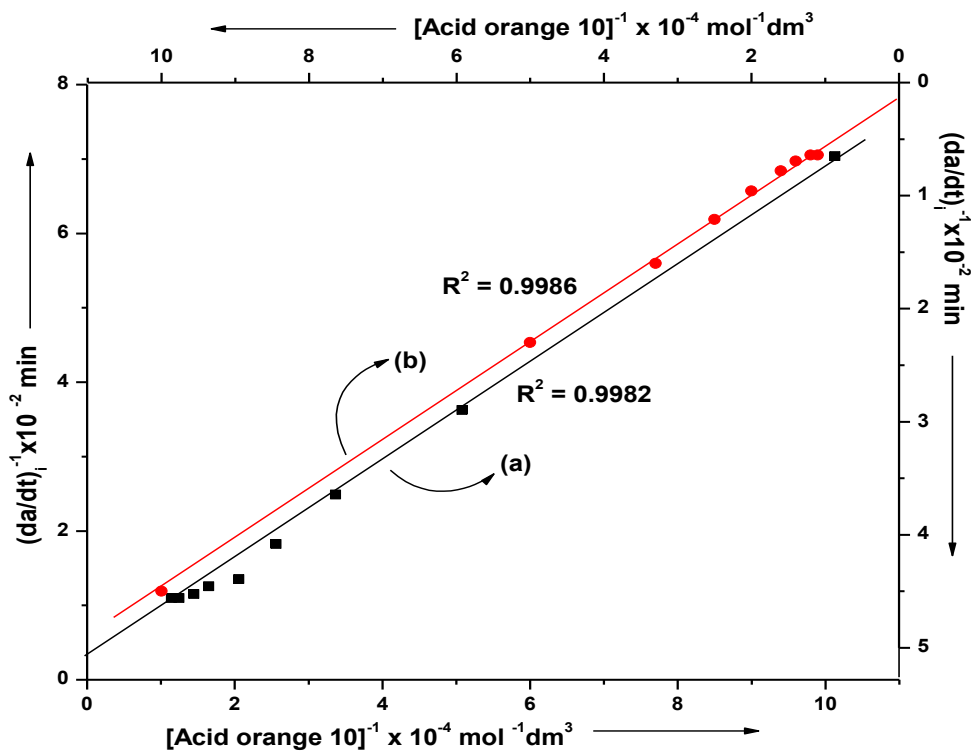
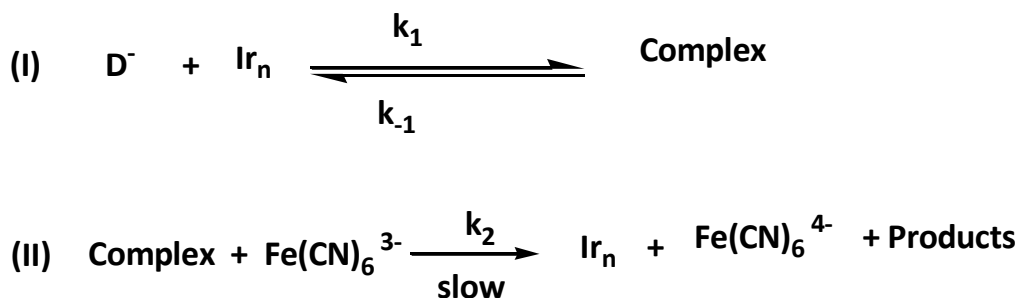


Fig. 14: Plot of rate⁻¹ vs [Acid orange 10]⁻¹





Scheme 2: Reaction mechanism for degradation of acid orange 10

non-zero intercept on the plot of 1/rate versus 1/[Substrate] (Figs. 13,14).

Rate Law

Based on the above mechanism and experimental facts, the following rate law has been derived:

$$-d[D^-]/dt = \frac{k_1 k_2 [D^-] [HCF(III)][Ir_n]_T}{k_{-1} + k_2 [HCF(III)] + k_1 [D^-]} \quad (1)$$

The rate law shows Pseudo first-order kinetics concerning Ir_n as well as retarding trend to HCF(III) and [D⁻].

At very low concentrations of HCF(III) ions and organic substrate, the value of k₂[HCF(III)] and k₁[D⁻] will be quite small. Hence neglecting these factors in the denominator, equation (1)

$$-d[D^-]/dt = \frac{k_1 k_2 [D^-][HCF(III)][Ir_n]_T}{k_{-1}} \quad (2)$$

Equation (2) accounts for the first-order kinetics concerning [HCF(III)], [D⁻], and the catalyst at their lower concentration. Equation (1) at constant

$$-d[D^-]/dt = \frac{k_1 k_2 [D^-] [HCF(III)]}{k_{-1} + k_2 [HCF(III)] + k_1 [D^-]} \quad (3)$$

For the verification of rate law at higher concentration equation (3) can be written as -

$$1/\text{rate} = \frac{k_{-1}}{k_1 k_2 [D^-] [HCF(III)]} + \frac{1}{k_1 [D^-]} + \frac{1}{k_2 [HCF(III)]} \quad (4)$$

According to equation (4), plots of 1/rate versus 1/[substrate], 1/rate versus 1/[HCF(III)] were found linear. Such plots are presented in Figs. 13 & 14. A close examination of these figures indicates that these are straight lines with positive intercepts at the 1/rate axis showing the validity

of the derived rate law equation based on the proposed mechanism.

CONCLUSION

Acid orange 10 is one of the most stable azo dyes which is extensively used in the textile industry and is resistant to biodegradation. This study demonstrates the effectiveness of the PVP and Brij stabilized IrO₂ nanoclusters in the degradation of acid orange 10. This study provides a comprehensive comparison between polyvinylpyrrolidone (PVP) and Brij-35 stabilized nanoclusters as catalysts for the degradation of Acid Orange 10. Both catalysts exhibited high activity and stability, with PVP-stabilized nanoclusters showing slightly higher activity. The PVP and Brij stabilized IrO₂ nanoclusters synthesized by the wet chemical method exhibited fast catalytic properties and reduced acid orange 10 to carboxylic acids. The dye degradation rates were very sensitive to pH and worked best at pH 8. The rate of degradation increased linearly with an increase in the concentration of HCF(III) and catalysts while the order of the reaction was found to be one at a lower concentration of dye tending towards zero at its higher concentration. The derived rate law supported the degradation mechanism. The catalytic activity of the PVP-stabilized IrO₂ nanoclusters was the highest among the three catalysts (PVP-stabilized IrO₂ nanoclusters, Brij-35 stabilized IrO₂ nanoclusters, and IrCl₃) used. The PVP-stabilized IrO₂ nanoclusters were repeatedly used over 3 cycles without significant loss of catalyst mass; a decrease in reaction rate constants is apparently due to the persistent agglomeration of IrO₂ nanoclusters after each cycle. Further, the degradation products analyzed by LC-MS were simpler and less hazardous. This is a novel approach to the



degradation process, which could potentially be more efficient and cost-effective than more traditional methods. Additionally, this study also provides a comparative analysis of the catalytic performance of these nanoclusters compared to other catalysts, allowing for a more comprehensive evaluation of the material's effectiveness. Finally, the study provides a detailed discussion of the mechanism of action and potential applications for these nanoclusters, which further enhances the value of the study.

CONFLICT OF INTEREST

The authors hereby declare that there is no conflict of interest.

REFERENCES

- Xue, H; S. Xiong, K. Mi and Y. Wang, 2023. Visible-light degradation of azo dyes by imine-linked covalent organic frameworks. *Green Energy Environ*, 8(1):194-199. <https://doi.org/10.1016/j.gee.2020.09.010>
- Yaseen D.A. and M. Scholz, 2019. Textile dye wastewater characteristics and constituents of synthetic effluents: a critical review. *Int. J. Environ. Sci. Technol*, 16:1193-1226. <https://doi.org/10.1007/s13762-018-2130-z>
- Najafi, M; T.R. Bastami, N. Binesh, A. Ayati and S. Emamverdi, 2022. Sono-sorption versus adsorption for the removal of congo red from aqueous solution using NiFeLDH/Au nanocomposite: Kinetics, thermodynamics, isotherm studies, and optimization of process parameters. *J Ind Eng Chem*, 116:489-503. <https://doi.org/10.1016/J.IJEC.2022.09.039>
- Omran, E; A. Ahmadi, M. Heravi and T.R. Bastami, 2022. Novel ZnTi LDH/h-BN nanocomposites for removal of two different organic contaminants: Simultaneous visible light photodegradation of Amaranth and Diazepam. *J Water Process Eng*, 47:102581. <https://doi.org/10.1016/j.jwpe.2022.102581>
- Cuerda-Correa, E.M; M.F. Alexandre-Franco and C. Fernández-González, 2020. Advanced oxidation processes for the removal of antibiotics from water. An overview. *Water*, 12:102. <https://doi.org/10.3390/w12010102>
- Ledakowicz, S and K. Pázdziór, 2021. Recent achievements in dyes removal focused on advanced oxidation processes integrated with biological methods. *Molecules*, 26(4):870. <https://doi.org/10.3390/molecules26040870>
- Augugliaro, V; M. Litter, L. Palmisano and J. Soria, 2006. The combination of heterogeneous photocatalysis with chemical and physical operations: A tool for improving the photoprocess performance. *J Photochem Photobiol C Photochem Rev*, 7:127-144. <https://doi.org/10.1016/j.jphotochemrev.2006.12.001>
- Javaid, R and U.Y. Qazi, 2019. Catalytic Oxidation Process for the Degradation of Synthetic Dyes: An Overview, 16(11):2066. <https://doi.org/10.3390/ijerph16112066>
- Xu, X.R; H.B. Li, W.H. Wang and J.D. Gu, 2005. Decolorization of dyes and textile wastewater by potassium permanganate. *Chemosphere*, 59:893-898. <https://doi.org/10.1016/J.CHEMOSPHERE.2004.11.013>
- Daneshvar, N; H. Ashassi Sorkhabi and M.B. Kasiri, 2004. Decolorization of dye solution containing Acid Red 14 by electrocoagulation with a comparative investigation of different electrode connections. *J Hazard Mater*, 112:55-62. <https://doi.org/10.1016/J.JHAZMAT.2004.03.021>
- Galindo, C; P. Jacques and A. Kalt, 2001. Photooxidation of the phenylazonaphthol AO20 on TiO₂: kinetic and mechanistic investigations. *Chemosphere*, 45:997-1005. [https://doi.org/10.1016/S0045-6535\(01\)00118-7](https://doi.org/10.1016/S0045-6535(01)00118-7)
- Konstantinou, I.K. and T.A. Albanis, 2004. TiO₂-assisted photocatalytic degradation of azo dyes in aqueous solution: kinetic and mechanistic investigations: A review. *Appl Catal B Environ*, 49:1-14. <https://doi.org/10.1016/J.APCATB.2003.11.010>
- Rahman, N; Z. Abedin and M.A. Hossain, 2014. Rapid degradation of azo dyes using nano-scale zero valent iron. *Am J Environ Sci*, 10:157-163. <https://doi.org/10.3844/ajessp.2014.157.163>
- Bhatti, H.N; Z. Iram, M. Iqbal, J. Nisar and M.I. Khan, 2020. Facile synthesis of zero valent iron and photocatalytic application for the degradation of dyes. *Mater Res Express*, 7: 015802. <https://doi.org/10.1088/2053-1591/ab66a0>
- Bokare, A.D; R.C. Chikate, C.V. Rode and K.M. Paknikar, 2008. Iron-nickel bimetallic nanoparticles for reductive degradation of azo dye Orange G in aqueous solution. *Appl. Catal. B Environ.*, 79:270-278. <https://doi.org/10.1016/j.apcatb.2007.10.033>
- Goel, A. and R. Lasyal, 2016. Iridium nanoparticles with high catalytic activity in degradation of acid red-26: An oxidative approach. *Water Sci. Technol.*, 74:2551-2559. <https://doi.org/10.2166/wst.2016.330>
- Jiang, J.Q. and B. Lloyd, 2002. Progress in the development and use of ferrate(VI) salt as an oxidant and coagulant for water and wastewater treatment. *Water Res*, 36:1397-1408. [https://doi.org/10.1016/S0043-1354\(01\)00358-X](https://doi.org/10.1016/S0043-1354(01)00358-X)
- Sen, F.G; A. Kinaci, B. Narayanan, S. K. Gray, M. J. Davis, S. K. R. S. Sankaranarayanan and M. K. Y. Chan, 2015. Towards accurate prediction of catalytic activity in IrO₂ nanoclusters via first principles-based variable charge force field. *J Mater Chem A*, 3:18970-18982. <https://doi.org/10.1039/C5TA04678E>
- Daiane Ferreira da Silva, C; F. Claudel, V. Martin, et al, 2021. Oxygen Evolution Reaction Activity and Stability Benchmarks for Supported and Unsupported Electrocatalysts. *ACS Catal*, 11:4107-4116. <https://doi.org/10.1021/acscatal.0c04613>
- Goel, A. and N. Rani, 2012. Effect of PVP, PVA and POLE surfactants on the size of iridium nanoparticles. *Open J Inorg Chem*, 02:67-73. <https://doi.org/10.4236/ojic.2012.23010>
- Lasyal, R. and A. Goel, 2018. Facile synthesis of nanoclusters and their application as catalysts in the degradation of azo dyes. *Turkish J Chem*, 42:941-957. <https://doi.org/10.3906/kim-1707-62>
- Sun, S.P; C.J. Li, J.H. Sun, S. H. Shi, M.H. Fan and Q. Zhou, 2009. Decolorization of an azo dye Orange G in aqueous solution by Fenton oxidation process: Effect of system parameters and kinetic study. *J Hazard Mater*, 161:1052-1057. <https://doi.org/10.1016/j.jhazmat.2008.04.080>
- Chang, M.C; H.Y. Shu, T.H. Tseng, H.W. Hsu, 2013. Supported Zinc Oxide Photocatalyst for Decolorization and Mineralization of Orange G Dye Wastewater under UV365 Irradiation. *Int J Photoenergy*, 2013: 595031. <https://doi.org/10.1155/2013/595031>

